Available online at www.sciencedirect.com

ScienceDirect

journal homepage: www.elsevier.com/locate/nanoenergy

nano energy
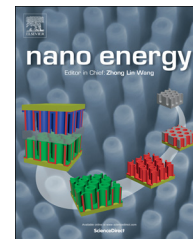
RAPID COMMUNICATION

Reducing CO_2 to dense nanoporous graphene by Mg/Zn for high power electrochemical capacitors

CrossMark

Zhenyu Xing[a],[1], Bao Wang[a],[1], Wenyang Gao[e], Changqing Pan[c],
Joshua K. Halsted[a], Elliot S. Chong[a], Jun Lu[b], Xingfeng Wang[a],
Wei Luo[a], Chih-Hung Chang[c], Youhai Wen[d], Shengqian Ma[e],
Khalil Amine[b],*, Xiulei Ji[a],*

[a]Department of Chemistry, Oregon State University, Corvallis, OR 97331, United States
[b]Argonne National Laboratory, Lemont, IL 60439, United States
[c]School of Chemical, Biological and Environmental Engineering, Oregon State University, Corvallis, OR 97331, United States
[d]National Energy Technology Laboratory, Albany, OR 97321, United States
[e]Department of Chemistry, Tampa, FL 33620, United States

Abstract
Converting CO_2 to valuable materials is attractive. Herein, we report using simple metallothermic reactions to reduce atmospheric CO_2 to dense nanoporous graphene. By using a Zn/Mg mixture as a reductant, the resulted nanoporous graphene exhibits highly desirable properties: high specific surface area of 1900 m^2/g, a great conductivity of 1050 S/m and a tap density of 0.63 g/cm^3, comparable to activated carbon. The nanoporous graphene contains a fine mesoporous structure constructed by curved few-layer graphene nanosheets. The unique property ensemble enables one of the best high-rate performances reported for electrochemical capacitors: a specific capacitance of ~170 F/g obtained at 2000 mV/s and 40 F/g at a frequency of 120 Hz. This simple fabricating strategy conceptually provides opportunities for materials scientists to design and prepare novel carbon materials with metallothermic reactions.
© 2014 Elsevier Ltd. All rights reserved.

*Corresponding authors.
E-mail addresses: amine@anl.gov (K. Amine),
david.ji@oregonstate.edu (X. Ji).
[1]These authors equally contributed to the paper.

Introduction

Fossil fuel combustion still represents the primary energy source for electricity generation around the globe. This process generates a tremendous amount of CO_2 that is considered as a primary contributor to the global climate change. It is highly desirable to utilize the abundant and wasteful CO_2 as a feedstock gas to synthesize valuable chemicals. Photocatalysis and hydrogenation have been shown effective to turn CO_2 into small organic molecules, such as HCOOH and CH_3OH [1-3]. However, few studies have focused on reducing CO_2 into functional carbonaceous materials. Herein, we aim to covert CO_2 into a dense nanoporous graphene as an electrode in high-power electrochemical capacitors (ECs).

ECs directly store electric energy via electrostatic attraction between the electrons or electron deficiencies on the electrode surface and the solvated ions in a liquid electrolyte, thus forming an electrical double layer on each electrode of ECs [4-8]. One of ECs' challenges is the low energy density, much less than the state-of-the-art batteries [7]. Currently, much attention is focused to improve ECs' energy density to a battery level without compromising power and cycle life [8]. Extensive efforts have been devoted to increasing capacitance of carbon materials that is governed by many factors, including surface area, conductivity, edge effect and porous structure [9-11]. Simultaneous optimization of all these factors has been very challenging. Another approach is to utilize non-diffusion-controlled redox reactions of nanosized metal oxides [12-19]. ECs are attractive mostly due to its much higher power density than batteries [10,11,20-22]. ECs can be fully charged in minutes or even seconds; however, this timeframe is still orders of magnitude longer than the time needed to charge conventional electrolytic capacitors [23]. At an ac frequency of 120 Hz, ECs behave almost like a pure resistor rather than a capacitor. The low conductivity of activated carbons (ACs), ~ 10 S/m to ~ 100 S/m, as electrodes in commercial ECs, is partially responsible for the poor high-frequency performance. Note that ACs can certainly exhibit high capacitance at intermediate current rates [24-26]. In order to further push the power of ECs to a higher level, more conductive electrode materials are highly demanded.

Recently, graphene materials attract intense attention for their applications as electrodes in ECs due to their high theoretical surface area of 2630 m^2/g and high theoretical conductivity [27,28]. In particular, graphene electrodes formed by chemical vapor deposition (CVD) demonstrated an excellent high-frequency performance for voltage filtering purposes. However, the volumetric capacitance of this type of graphene is low, which may prevent it from being used for energy storage applications [29,30]. Therefore, it is highly desirable to synthesize a nanoporous graphene with a large surface area and a great conductivity while exhibiting a high density. Currently, the primary synthetic strategy of nanoporous graphene is via the Hummer's method that first exfoliates graphite into graphene oxide via an intense oxidation process [31,32,33]. Different reduction approaches for graphene oxide have been reported, including chemical reduction [34], KOH activation [35], solvation [36,37], solvothermal reduction [38,39], thermal reduction [40,41], microwave heating [42], light irradiation [43-45] and graphene crumping [46]. Excellent energy and power densities of ECs have been reported [47-49]. However, the syntheses based on the Hummer's method have to use highly corrosive oxidizing reagents, i.e., concentrated H_2SO_4 and $KMnO_4$, and labor-intensive purification procedures, which raises the cost and limits the scalability of the graphene production [50]. Therefore, it is highly desirable to investigate fundamentally new methodologies to prepare high quality nanoporous graphene in a cost-effective and scalable manner.

Herein, we convert atmospheric CO_2 into nanoporous graphene via simple metallothermic reactions. In particular, magnesiothermic reactions are well known for their capability in dissociating robust chemical bonds, including the Si-O bond in SiO_2 in forming nanoporous silicon and the C-O bond in reducing graphene oxides [51,52]. Xu and Lu et al. first observed few-layered graphene formed in the magnesium combustion reaction with dry ice [7,53]. Most recently, Pumera et al. reported that reducing CO_2 by lithium metal forms graphene materials as well [54]. Huczko et al. reduced CO_2 by a few different metals into carbon materials [55]. Ma et al. investigated a burn-quench method to reduce CO_2 by Mg as well as studied magnesiothermic reduction of CO_2 at different temperatures [56,57].

With Mg or Mg/Zn mixture as the reductant, we reduced atmospheric CO_2 to nanoporous graphene with various graphitization degrees and specific surface areas. The Mg/Zn reduced graphene demonstrates a specific capacitance of ~ 170 F/g even at a sweeping rate of 2000 mV/s in cyclic voltammetry (CV) measurements and a capacitance of 40 F/g at an ac frequency of 120 Hz extrapolated from the electrochemical impedance spectroscopy (EIS) results.

Experimental

Preparation of nanoporous graphenes

In a typical experiment, 1.5 g of Mg powder or Mg powder well mixed with different amounts of Zn powder was placed in an Al_2O_3 boat and heated in a tube furnace at 680 °C under a CO_2 flow at 70 cm^3/min (CCM) for 60 min. After the reaction, the black product was collected and stirred in 2.0 M HCl solution at room temperature for 10 h to remove the MgO (and ZnO). The mixture was then filtered and washed with deionized water several times until the filtrate exhibits a pH value, around 6. Finally, ethanol was used to rinse the isolated solid carbon product before drying at room temperature overnight.

Characterization methods

X-Ray diffraction (XRD) patterns were recorded by using a Rigaku Ultima IV Diffractometer with Cu Kα irradiation ($\lambda = 1.5406$ Å). A WITec confocal Raman spectrometer with a 514 nm laser source was employed to collect the Raman spectra. The morphology was studied by field emission scanning electron microscopy (FESEM) using an FEI NOVA 230 high resolution SEM with an energy-dispersive X-ray (EDX) attachment. Transmission electron microscopy (TEM) images were recorded by FEI Titan 80-200 TEM. High-angle annular dark field scanning TEM (HAADF-STEM) measurements were carried out on an FEI Titan 80-200 microscope

coupled with a HAADF detector and an EDX spectrometer. Nitrogen sorption measurements were performed on Micromeritics TriStar II 3020 analyzer.

Electrode preparation of ECs

Electrodes were composed of 80 wt% C-M or C-MZ, 10 wt% carbon additive (Super P) and 10 wt% poly(vinylidene fluoride) (PVDF) binder. The electrode mixture was brushed from a cyclopentanone slurry onto a stainless steel current collector (stainless steel gauze, 80 mesh) before the electrodes were dried at 120 °C under vacuum for 12 h. Typical active mass loading is 1.6 mg/cm^2.

Electrochemical measurements

A two-electrode cell configuration was employed to measure the electrochemical performance. We used coin-type cells that contain two nearly identical electrodes (by weight and size) loaded onto two current collectors, respectively. In between the electrodes, a piece of Whatman$^{®}$ filter paper is used as the cell separator. The electrolyte is a 6.0 M KOH aqueous solution. A VMP-3 multi-channel workstation was used for CV measurements, galvanostatic charge/discharge (CD) cycling and EIS tests. Specific capacitance was estimated from galvanostatic cycling by using the formula:

$$C = 4I \cdot \Delta t / (m \cdot \Delta V) \quad (1)$$

[35] where I is the applied current, Δt refers to the discharge time, and m is the total mass for both electrodes, and ΔV represents the voltage drop of discharging curve. The EIS tests were carried out at room temperature at the frequency range of 200 kHz to 10 mHz.

Effective series resistance (ESR) was estimated with the following equation:

$$R_{ESR} = V_{drop} / (2I) \quad (2)$$

[35] where, V_{drop} is the voltage drop at the beginning of the discharge curve at a certain constant current density, I.

The specific power was calculated by the following formula:

$$P = (V_{max} - V_{drop})^2 / (4mR_{ESR}) \quad (3)$$

[35] where V_{max} is the cutoff voltage at the beginning of the discharge and V_{drop} is the initial vertical drop of the voltage.

Based on the EIS results, the capacitance was also calculated using the following equation:

$$C = \frac{-1}{2\pi f z''} \quad (4)$$

[35] where f is the frequency (Hz) and Z'' is the imaginary part of the impedance.

Results and discussion

In a typical experiment, Mg powder was placed in a ceramic boat and heated in a tube furnace at 680 °C under a CO_2 flow rate of 70 CCM for 60 min. The carbon formation reaction can be described by the following equation:

$$CO_2 \ (g) + 2Mg \ (l) \rightarrow C \ (s) + 2MgO \ (s) \quad (5)$$

Much heat should be emitted from the above reaction as the Gibbs free energy of the above reaction is calculated to be −608 KJ/mol at 680 °C. We expect that the reaction temperature is much higher than the set temperature for the furnace. In order to estimate the 'real' reaction temperature, we mixed different metal carbonates with Mg powder in the reaction, namely $SrCO_3$ or $BaCO_3$ that decomposes at 1100 °C and 1450 °C, respectively. After the reaction, SrO phase was identified in the product, indicating that the reaction temperature is higher than 1100 °C. We did not observe BaO in the product; therefore, the reaction temperature is no higher than 1450 °C (Supplementary Figure S1).

Another fundamental question of the reaction is whether Mg vapor or molten Mg acts as the reducing phase for CO_2. In order to answer this question, we heated an MgO pellet atop an Mg pellet under CO_2. After the reaction, the Mg pellet turned black with its pellet shape well retained while the MgO pellet remained white (Figure 1). The lack of carbon formed
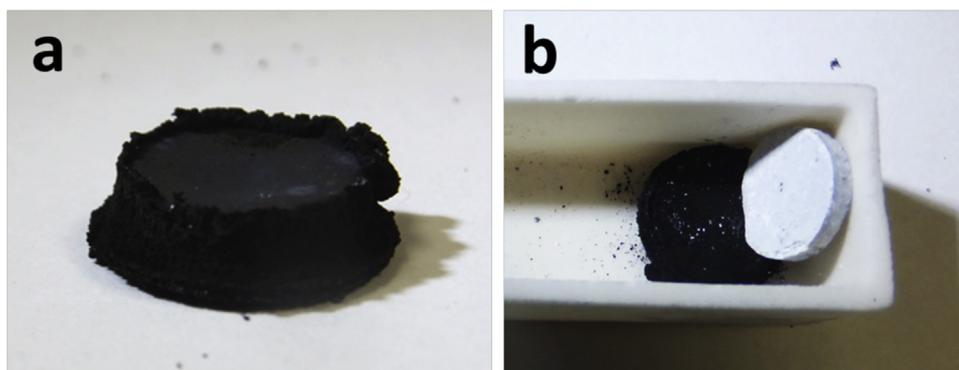
Figure 1 Digital images of pellet of Mg or Mg/MgO after annealing under CO_2, indicating that Mg cannot be evaporated under CO_2 reduction. (a) An Mg pellet after the reaction at 680 °C and 70 CCM CO_2 flow rate in one hour. (b) An MgO pellet stacked on an Mg pellet after a reaction at the same conditions as above. The MgO pellet is flipped upright to show its side that touched the Mg pellet during the reaction.
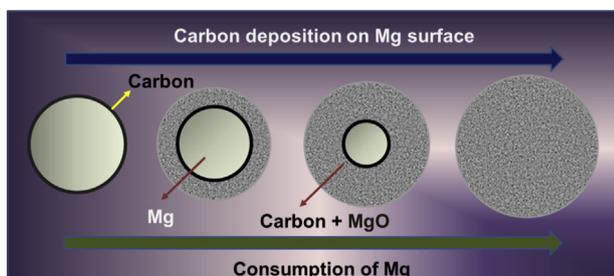
Figure 2 Schematic diagram illustrates the carbon deposition at the surface of molten Mg droplet at the expense of Mg phase along the reaction.

on the surface of the MgO pellet suggests that Mg cannot be evaporated under CO_2 due to the rapid Mg/CO_2 reactions. It is also reasonable to assume that CO_2 molecules cannot diffuse into the molten Mg droplets either. Therefore, we postulate that it is the molten Mg surface where CO_2 is reduced to solid carbon. During the reaction, an MgO/C nanocomposite is formed at the expense of Mg phase, as schematically proposed in Figure 2.

Based on the above proposed mechanism, we hope to control the properties of the as-formed carbon by varying experimental conditions. We focused our attention on graphitization degrees and specific surface area, the two properties that are most relevant to the performance in ECs. We refer to reaction products here as C-Ms. The intensive peaks in X-ray diffraction (XRD) patterns indicate that nearly all C-Ms comprise well-crystalized graphite domains except for the product formed at 650 °C (Figure 3a,d,g). We evaluate the graphitization degrees by the ratios between D and G bands (I_D/I_G) at 1340 cm^{-1} and 1570 cm^{-1}, respectively, in Raman spectra of the products [58]. The D and G band correspond to the defective sp^2 structure and the graphene in-plane vibrations in carbon materials, respectively. Additionally, if 2D-band at 2645 cm^{-1} shows up, it also indicates a high graphitization degree of the product. By comparing spectra in Figure 3b,e,h, we notice that the graphitization degree of products increases from 650 to 680 °C but decreases at 710 °C. The reaction duration also affects the graphitization degree. The highest graphitization degree is achieved after the reaction for one hour. A similar trend is observed with the CO_2 flow rate as well. The graphitization degree rises upon increasing the CO_2 flow rate from 25.5 CCM to 70 CCM but decreases at 229 CCM.

The above results reflect CO_2's dual-role in the reaction in terms of carbon formation and activation (gasification). Note that CO_2 can etch the as-formed carbon in the following reaction:

$$CO_2 \text{ (g)} + C \text{ (s)} \rightarrow 2CO \text{ (g)} \qquad (6)$$

Note that the best graphitization degree and highest Brunauer-Emmett-Teller (BET) specific surface area of 829 m^2/g were achieved simultaneously at 680 °C and a CO_2 flow rate of 70 CCM after one hour (Figure 3c,f,i and Supplementary Figure S2a-k).

We also studied the CO_2 reduction with pure Zn as a reductant but found that no black carbon was formed after the reaction simply by visual inspection, although Zn was oxidized to ZnO, as revealed by the XRD pattern of the solid product (Supplementary Figure S3). We calculated the

energetics for the reaction between $CO_2 + Zn$, and found out that the mixture of graphite and ZnO are thermodynamically unstable at a temperature above 904 °C as they will react to produce CO (gas) and Zn (gas). We hypothesize that Zn vapor generated at this temperature during the magnesiothermic reactions may enhance the nanoporosity of the graphene products. The carbons reduced by Zn/Mg mixtures are referred to as C-MZ-n, where n indicates the molar ratio between Zn and Mg in the reductant mixture.

The specific surface area of C-MZ-n was, indeed, dramatically increased, compared to C-Ms, reaching a plateau of ~ 1900 m^2 when the Zn/Mg ratio is three or above (Figure 4c). Furthermore, all C-MZs exhibit much diminished graphite crystalline features, compared to C-Ms, as evident by the much less resolved XRD peaks and higher I_D/I_G ratios in Raman spectra (Figure 4a,b).

We examined the nanoporosity of C-M and a representative C-MZ-n, C-MZ-3, by transmission electron microscopy (TEM). As Figure 5a implies, C-M exhibits a porous structure. Under a higher magnification, it is evident that the voids in C-M are in between crystalline graphite nanodomains with (002) lattice fringes displayed (Figure 5c). In sharp contrast, C-MZ-3 comprises highly populated smaller nanopores with a uniform pore size distribution (PSD), as shown in Figure 5b. As shown in the zoomed-in image (Figure 5d), it is evident that curved few-layer graphene-nanosheets construct C-MZ-3's highly nanoporous structure. There are less than 10 layers spanning in the nanowalls; therefore, we choose to refer to this carbon as nanoporous graphene [59]. This represents a rarely observed scenario that high specific surface area and highly graphitic nanostructure are integrated in one carbon material. The structural contrast between a typical amorphous nanoporous carbon and C-MZ-3 is demonstrated in Figure S4. C-MZ-3 exhibits a slightly lower conductivity of 1050 S/cm than C-M, 1180 S/cm, but this conductivity is still ten times higher than that of conventional activated carbons, which indicates the fact that fine nanoporosity may not interrupt the effective electronic percolation.

We collected N_2 isotherms and Density Functional Theory (DFT) PSD for all the CO_2-derived nanoporous graphene materials, as Figure S2 displays. N_2 isotherms of C-Ms (Figure S2a-k) contain a hysteresis over a wide pressure range, particularly at high relative pressures, indicating a large range of nanopore sizes and a good population of big nanopores, 4-12 nm in size. Interestingly, all C-Ms exhibit a bimodal PSD with pore sizes centered near 7 and 9 nm, respectively. On the other hand, the isotherms of C-MZ-n (Supplementary Figure S2l-r) also display a hysteresis; however, different from C-Ms, C-MZ-n adsorbs a large volume of N_2 at very low relative pressures. This is more obvious when the Zn/Mg atomic ratio is equal or higher than 3. The high adsorption at low pressures suggests the existence of a large population of small nanopores, i.e., micropores (< 2 nm). The PSD curves of C-MZ-n reveal that the majority of the nanopores in C-MZ-n are less than 4 nm. Most C-MZ-n's structures are multi-modal with spikes in PSD below 2 nm. The clear variance in PSD between C-Ms and C-MZ-n can only be attributed to the addition of Zn into the reductant.

We attempted to elucidate the porosity-formation mechanism in C-Ms and C-MZ-n. For C-Ms, it is reasonable
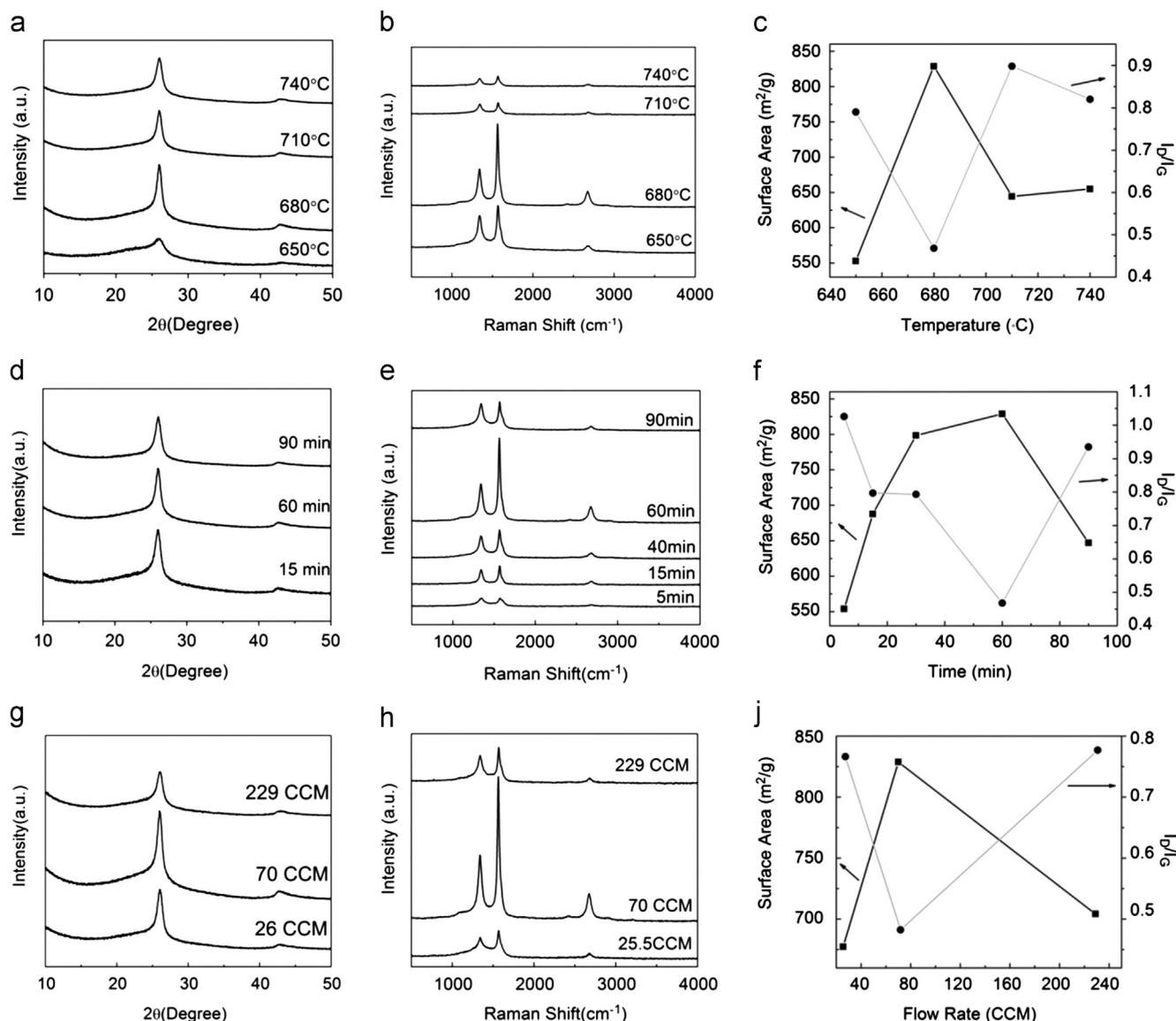
Figure 3 XRD patterns and Raman spectra of the C-Ms demonstrate different degrees of graphitization and specific surface areas upon various reaction conditions. (a,b) At different temperatures but a fixed a CO_2 flow rate of 70 CCM after a fixed reaction duration of one hour. (d,e) After different reaction durations at a fixed CO_2 flow rate of 70 CCM and at a fixed temperature of 680 °C. (g,h) At different CO_2 flow rates at a fixed temperature of 680 °C after a fixed reaction duration of one hour. (c,f,i) Specific surface areas and I_D/I_G ratios of the C-Ms in Raman spectra as a function of different reaction temperatures, reaction durations and flow rates, respectively. The optimal graphitization and highest surface area are achieved simultaneously at 680 °C and a CO_2 flow rate of 70 CCM after one hour of reaction.

to believe that MgO removal results in the formation of large nanopores. A high angle angular dark field (HAADF) scanning TEM image and the corresponding EDX elemental mapping reveal that Mg element homogeneously occupies space in the product obtained after CO_2 reduction by Mg (Figure S5). Similarly, both Mg and Zn elements uniformly exist in the product with Mg/Zn as the reductant (Figure S6). For C-MZ-n, we postulate that Mg in the Mg/Zn mixture is responsible for the large nanopores, while Zn is responsible for the micropores. Under TEM, we observed some metal oxide nanoparticles in C-MZ-3 that survived the vigorous HCl acid treatment. These nanoparticles identify themselves as Wurtzite ZnO by selected area electron

diffraction patterns (SAED) (Figure 5e). We pay close attention to the boundary region between ZnO nanoparticles and the nearby phases. As shown in Figure 5f, on a ZnO nanoparticle that displays (100) lattice fringes, epitaxial growth of graphitic lattices is evident, where the (002) d-spacing increases from 3.1 Å to 3.3 Å, radiating away from the ZnO nanoparticle. Note that both Wurtzite ZnO and graphite exhibit hexagonal type of crystal structures while crystalline MgO is cubic, which implies that ZnO may act as a more efficient epitaxial substrate for graphene growth than MgO. ZnO nanoparticles get covered by graphene more rapidly, thus preventing metal oxide particles from further growth.
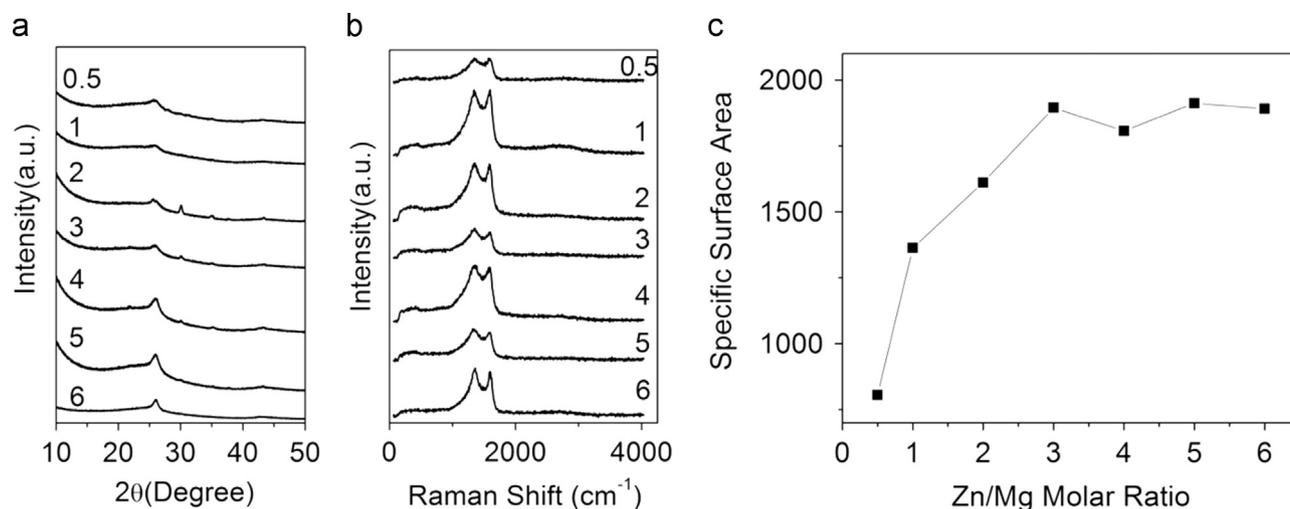
Figure 4 XRD patterns and Raman spectra of the C-MZ-*n* revealing less crystalline graphitic structures. (a) XRD patterns and (b) Raman spectra of C-MZ-*n* formed by different Zn/Mg molar ratios. (c) Surface area of C-MZ-*n* as a function of Zn/Mg molar ratio.

We investigated, in two-electrode symmetric cells, the electrochemical power performance of the CO_2-derived nanoporous carbons in ECs. Both C-M and C-MZ-3 are able to retain their capacitance upon dramatic increasing the potentiostatic sweeping rates or the galvanostatic current rates. As Figure S7a and Figure 6a show, both C-M and C-MZ-3 demonstrate capacitor-characteristic cyclic voltammetry (CV) curves even at a sweeping rate of 2000 mV/s, with only slightly decreased area enclosed in the nearly rectangular CV curves, demonstrating one of the best high-rate performances ever reported for carbon materials in ECs. In between C-M and C-MZ-3, C-MZ-3 exhibits a specific capacitance of 170 F/g at 2000 mV/s, much higher than ~60 F/g of C-M obtained at the same rate, mainly due to the higher surface area.

Galvanostatic charge/discharge (CD) measurements also confirm the fast chargeability of C-MZ-3 and C-M, as Figure 6b and Figure S7b show, respectively. At a current rate of 10 A/g, C-MZ-3 delivers a high specific capacitance of 190 F/g and very symmetrical triangular charge/discharge curves. The tiny voltage drop at the beginning of the discharge curve indicates a very low equivalent series resistance (ESR) of the cell due to the high conductivity of the graphene electrodes. The specific peak power density is calculated to be 197 KW/kg based on the ESR and the mass only from the carbon electrodes (see Supplementary), which is comparable to the power density exhibited by KOH-activated nanoporous graphene reduced from graphene oxide. Note that the electrodes only hold a part of the mass in practical supercapacitors as there are electrolyte, separator as well as current collectors that contribute to the total mass of the cells. Furthermore, C-MZ-3 also exhibits a very stable cycling life with more than 98% of the initial capacitance retained after 10,000 cycles (Supplementary Figure S8).

The electrochemical impedance spectra (EIS) corroborate the excellent electrical double layer behavior of C-MZ-3 and C-M, as revealed by CV and CD tests (Figure 6c,d and Figure S3c,d). The complex-plane Nyquist plot of C-MZ-3 displays a nearly vertical line with a semicircle in the high-frequency region. The high-frequency region is fit and simulated by an equivalent circuit, as shown in Figure 6c inset, where two RC circuits, an ESR and a restricted diffusion impedance element (M) are in series. The restricted diffusion impedance element indicates that the ion diffusion in electrolyte is much slower than the charge carrier mobility in the electrodes. Similar Nyquist plots were also observed on other graphene-based electrodes in ECs [35]. Furthermore, we plotted the specific capacitance as a function of ac frequency based on the EIS results. C-MZ-3 exhibits an impressive specific capacitance of 40 F/g even at 120 Hz, which corresponds to a discharge/charge cycle in 8.3 milliseconds, while it is only 3 F/g for best material among C-Ms. This high-rate performance of C-MZ-3 is comparable to the porous graphene prepared by KOH activation, reported by Ruoff et al. [35] and by laser irradiation, reported by Kaner et al. [44]. The Bode plots with the phase angle as a function of frequency for both Mg and Mg/Zn samples are shown in Figure S10. At a frequency of 1 Hz corresponding to charge/discharge cycle completed in 1 s, the phase angle for C-MZ is $-60°$ slightly higher than $-55°$ for C-M.

We pay close attention to the estimation of the volumetric capacitance of C-MZ-3 that will heavily affect the dimensions of ECs. Under a pressure of three ton per square inch, a pellet of C-MZ-3 exhibits a density 0.63 g/cm^3, comparable to that of commercial activated carbons. This nanoporous graphene may be one of the densest graphene materials reported. As shown by the SEM images in Figure S9, the bulk-sized morphology of C-M and C-MZ-3 also indicates their relatively high density. Based on the density of the nanoporous graphene and the estimated porosity of typical thin-film electrodes (~30 v%), C-MZ-3-based electrodes could potentially exhibit a volumetric capacitance of 70 F/cm^3 at 2000 mV/s and 17 F/cm^3 at 120 Hz, which is certainly superior to electrodes employing carbon nanotubes or most low-density graphene materials, and higher than activated carbons in commercial ECs when cycled at high current rates [60].

We also revealed the potential of scalability for this new preparation strategy. We increased the usage of Mg in the reaction from 1.5 g to 15 g, and the 10 times scaled-up reaction gives rise to the same product yield of slightly more than 40% with the same properties retained in specific surface area and conductivity. A very similar yield was observed for the syntheses of C-MZs. The 100% yield would
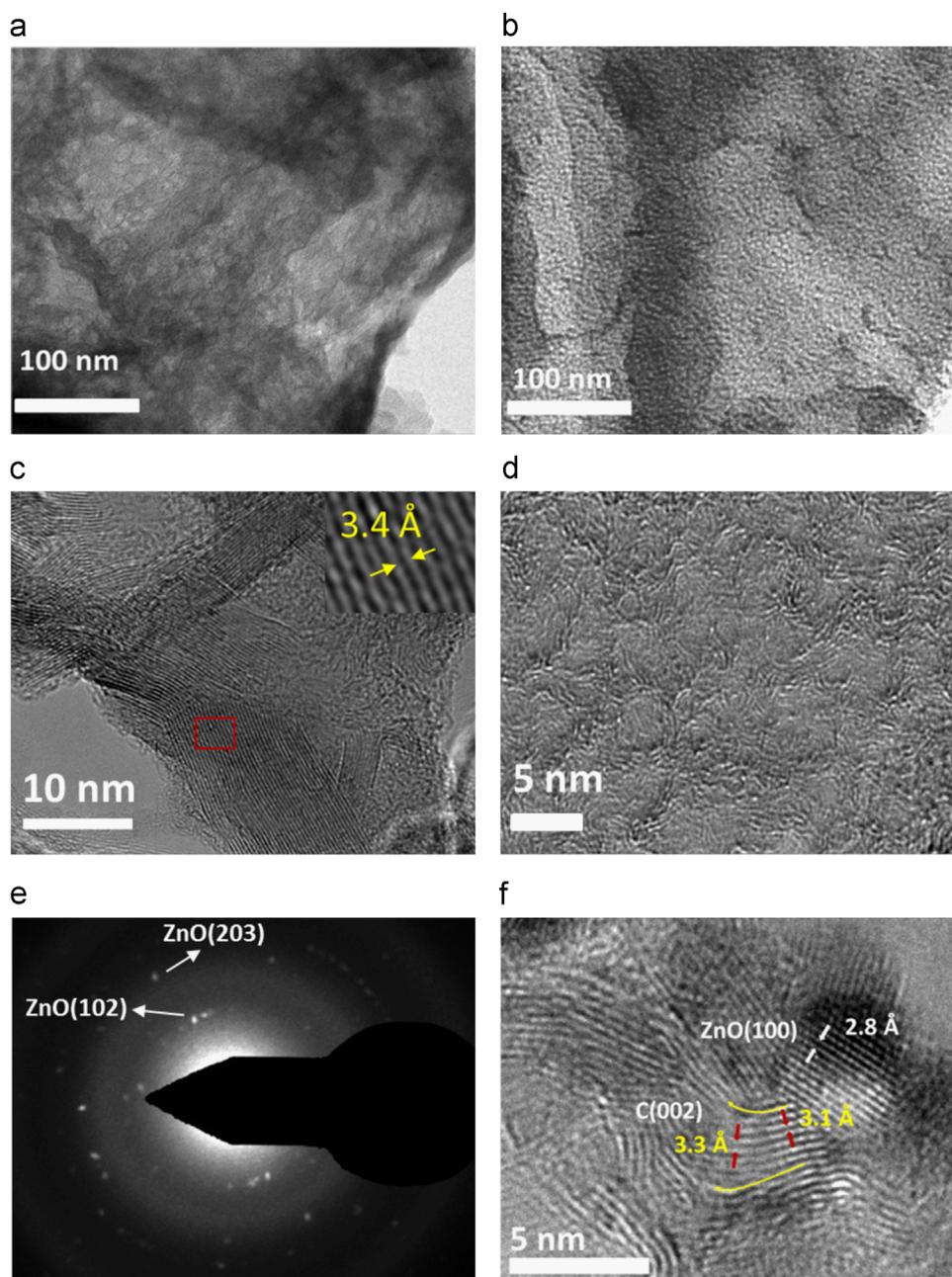
Figure 5 TEM images of C-M and C-MZ-3, revealing their different nanoporosity. (a,c) Low and high magnifiction images of C-M, and the inset in c is an enlarged image of the area marked by a red box. (b,d) Low and high magnifcation images of C-MZ. (e) SAED of C-MZ-3. (f) A representative ZnO nanoparticle in C-MZ-3, showing ZnO lattice fringes and graphene lattice epitaxially grown on the surface of ZnO with increasing graphitic (002) d-spacing radiating away from ZnO surface.

be obtained if we assume that Mg consumption in the reaction only results in carbon formation.

Furthermore, the potential practical application of this CO_2-derived nanoporous graphene in supercapacitors relies on its affordability. Mg and Zn metals are relatively cost-effective. In fact, Mg and Zn metal can be recycled after the reaction, which may lower the cost. Moreover, the reaction is exothermic where the heat energy could be collected for electricity generation, which may further decrease the cost. The preparation method is promising to be very competitive in terms of its high quality/cost values.

Conclusion

In summary, we have demonstrated that reducing abundant and wasteful atmospheric CO_2 by controlled metallothermic reactions is a viable strategy to synthesize superior nanoporous graphene as electrodes for high power electrochemical capacitors. The new synthetic strategy utilizes the inexpensive Mg and Zn as the reductant, which renders great affordability and scalability. The addition of Zn into the metal reductant has a significant impact on the properties of the obtained nanoporous graphene where the nanostructure is constructed by well-
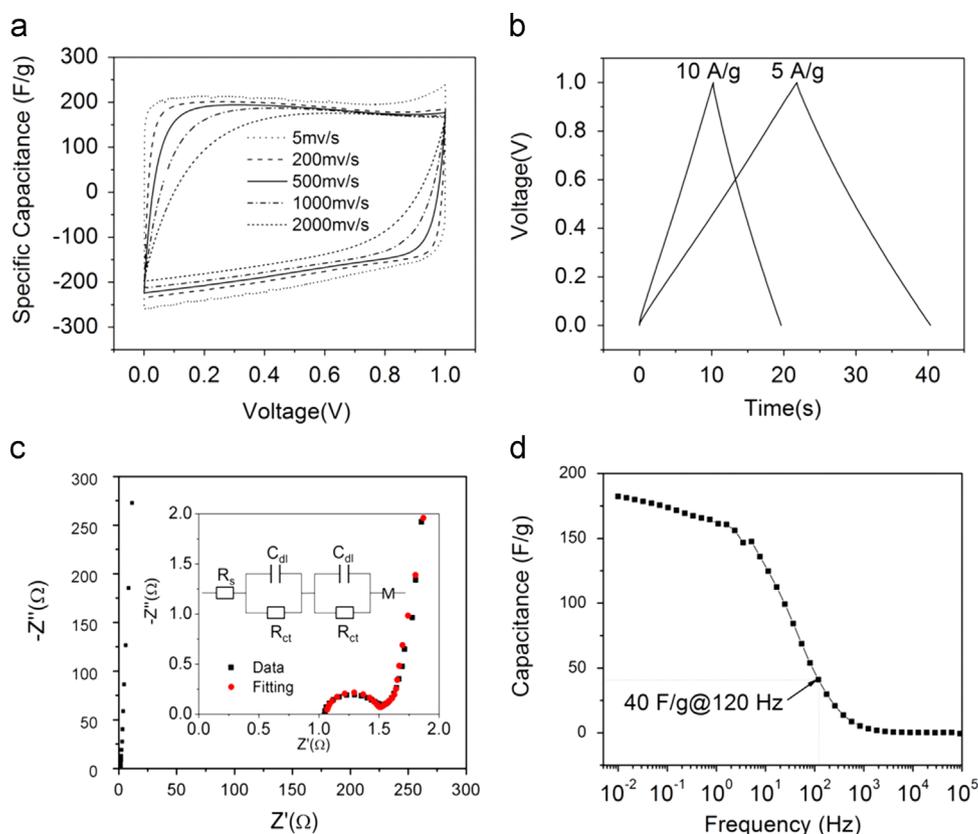
Figure 6 Electrochemical characterizations of C-MZ-3. (a) CV curves at different sweeping rates. The well-maintained rectangular CV curves at very high sweeping rates demonstrates the high rate capability. (b) Galvanostatic charge/discharge curves recorded at current densities of 5 A/g and 10 A/g. (c) Complex-plane Nyquist plot with the imaginary part as a function of the real part of impedance. Inset shows the expansion of the high frequency region and the equivalent circuit simulation. (d) Specific capacitance as a function of ac current frequency, revealing a specific capacitance of 40 F/g retained at a high ac frequency of 120 Hz marked.

resolved few-layer graphene nanosheets. The new strategy, for the first time, realizes, in one material, the three most needed properties for superior electrodes in supercapacitors: high specific surface area, high conductivity and relatively high density. The unique property ensemble enables one of the best high rate performances ever reported. We expect that both the preparation methodology and the obtained nanoporous graphene materials will generate a strong impact on the fields of carbon science and high power energy storage devices.

Acknowledgments

Appendix A.   Supporting information

Supplementary data associated with this article can be found in the online version at http://dx.doi.org/10.1016/j.nanoen.2014.11.011.

References

[1] G.A. Olah, G.K.S. Prakash, A. Goeppert, J. Am. Chem. Soc. 133 (2011) 12881-12898.
[2] S.C. Roy, O.K. Varghese, M. Paulose, C.A. Grimes, ACS Nano 4 (2010) 1259-1278.
[3] W. Leitner, Angew Chem. Int. Ed. 34 (1995) 2207-2221.
[4] M. Noked, A. Soffer, D. Aurbach, J. Solid State Electrochem. 15 (2011) 1563-1578.
[5] M.D. Levi, G. Salitra, N. Levy, D. Aurbach, J. Maier, Nat. Mater. 8 (2009) 872-875.
[6] Y.P. Zhai, Y.Q. Dou, D.Y. Zhao, P.F. Fulvio, R.T. Mayes, S. Dai, Adv. Mater. 23 (2011) 4828-4850.
[7] P. Simon, Y. Gogotsi, Nat. Mater. 7 (2008) 845-854.
[8] D. Pech, M. Brunet, H. Durou, P.H. Huang, V. Mochalin, Y. Gogotsi, P.L. Taberna, P. Simon, Nat. Nanotechnol. 5 (2010) 651-654.
[9] C. Merlet, B. Rotenberg, P.A. Madden, P.L. Taberna, P. Simon, Y. Gogotsi, M. Salanne, Nat. Mater. 11 (2012) 306-310.
[10] J. Chmiola, C. Largeot, P.L. Taberna, P. Simon, Y. Gogotsi, Science 328 (2010) 480-483.
[11] Q. Li, R.R. Jiang, Y.Q. Dou, Z.X. Wu, T. Huang, D. Feng, J.P. Yang, A.S. Yu, D.Y. Zhao, Carbon 49 (2011) 1248-1257.
[12] T. Brezesinski, J. Wang, S.H. Tolbert, B. Dunn, Nat. Mater. 9 (2010) 146-151.
[13] V. Augustyn, J. Come, M.A. Lowe, J.W. Kim, P.L. Taberna, S. H. Tolbert, H.D. Abruna, P. Simon, B. Dunn, Nat. Mater. 12 (2013) 518-522.

[14] L.Q. Mai, H. Li, Y.L. Zhao, L. Xu, X. Xu, Y.Z. Luo, Z.F. Zhang, W. Ke, C.J. Niu, Q.J. Zhang, Sci. Rep.-Uk 3 (2013) 1718. http://dx.doi.org/10.1038/srep01718.

[15] A.E. Fischer, K.A. Pettigrew, D.R. Rolison, R.M. Stroud, J.W. Long, Nano Lett. 7 (2007) 281-286.

[16] L.B. Hu, W. Chen, X. Xie, N.A. Liu, Y. Yang, H. Wu, Y. Yao, M. Pasta, H.N. Alshareef, Y. Cui, ACS Nano 5 (2011) 8904-8913.

[17] G.H. Yu, X. Xie, L.J. Pan, Z.N. Bao, Y. Cui, Nano Energy 2 (2013) 213-234.

[18] P.H. Yang, Y. Ding, Z.Y. Lin, Z.W. Chen, Y.Z. Li, P.F. Qiang, M. Ebrahimi, W.J. Mai, C.P. Wong, Z.L. Wang, Nano Lett. 14 (2014) 731-736.

[19] L. Huang, D.C. Chen, Y. Ding, S. Feng, Z.L. Wang, M.L. Liu, Nano Lett. 13 (2013) 3135-3139.

[20] J.R. Miller, P. Simon, Science 321 (2008) 651-652.

[21] J. Chmiola, G. Yushin, Y. Gogotsi, C. Portet, P. Simon, P.L. Taberna, Science 313 (2006) 1760-1763.

[22] W.J. Yuan, Y. Zhou, Y.R. Li, C. Li, H.L. Peng, J. Zhang, Z.F. Liu, L.M. Dai, G.Q. Shi, Sci. Rep.-Uk 3 (2013) 2248. http://dx.doi.org/10.1038/srep02248.

[23] J.R. Miller, A.F. Burke, Electrochem. Soc. Interface (2008), Spring, 53-57.

[24] Y. Korenblit, A. Kajdos, W.C. West, M.C. Smart, E.J. Brandon, A. Kvit, J. Jagiello, G. Yushin, Adv. Funct. Mater. 22 (2012) 1655-1662.

[25] L. Wei, M. Sevilla, A.B. Fuertes, R. Mokaya, G. Yushin, Adv. Energy Mater. 1 (2011) 356-361.

[26] J. Wei, D.D. Zhou, Z.K. Sun, Y.H. Deng, Y.Y. Xia, D.Y. Zhao, Adv. Funct. Mater. 23 (2013) 2322-2328.

[27] K.S. Novoselov, A.K. Geim, S.V. Morozov, D. Jiang, Y. Zhang, S.V. Dubonos, I.V. Grigorieva, A.A. Firsov, Science 306 (2004) 666-669.

[28] L.M. Dai, Acc. Chem. Res. 46 (2013) 31-42.

[29] Z.P. Chen, W.C. Ren, L.B. Gao, B.L. Liu, S.F. Pei, H.M. Cheng, Nat. Mater. 10 (2011) 424-428.

[30] J.R. Miller, R.A. Outlaw, B.C. Holloway, Science 329 (2010) 1637-1639.

[31] F. Zhang, T.F. Zhang, X. Yang, L. Zhang, K. Leng, Y. Huang, Y.S. Chen, Energy Environ. Sci. 6 (2013) 1623-1632.

[32] W.S. Hummers, R.E. Offeman, J. Am. Chem. Soc. 80 (1957) (1339-1339).

[33] D.C. Marcano, D.V. Kosynkin, J.M. Berlin, A. Sinitskii, Z.Z. Sun, A. Slesarev, L.B. Alemany, W. Lu, J.M. Tour, ACS Nano 4 (2010) 4806-4814.

[34] I.K. Moon, J. Lee, R.S. Ruoff, H. Lee, Nat. Commun. 1 (2010) 73. http://dx.doi.org/10.1038/ncomms1067.

[35] Y.W. Zhu, S. Murali, M.D. Stoller, K.J. Ganesh, W.W. Cai, P. J. Ferreira, A. Pirkle, R.M. Wallace, K.A. Cychosz, M. Thommes, D. Su, E.A. Stach, R.S. Ruoff, Science 332 (2011) 1537-1541.

[36] X.W. Yang, J.W. Zhu, L. Qiu, D. Li, Adv. Mater. 23 (2011) 2833−2838.

[37] X.W. Yang, C. Cheng, Y.F. Wang, L. Qiu, D. Li, Science 341 (2013) 534-537.

[38] M. Choucair, P. Thordarson, J.A. Stride, Nat. Nanotechnol. 4 (2009) 30-33.

[39] H.L. Wang, J.T. Robinson, X.L. Li, H.J. Dai, J. Am. Chem. Soc. 131 (2009) 9910-9911.

[40] S. Stankovich, D.A. Dikin, R.D. Piner, K.A. Kohlhaas, A. Kleinhammes, Y. Jia, Y. Wu, S.T. Nguyen, R.S. Ruoff, Carbon 45 (2007) 1558-1565.

[41] W. Gao, L.B. Alemany, L.J. Ci, P.M. Ajayan, Nat. Chem. 1 (2009) 403-408.

[42] Y.W. Zhu, S. Murali, M.D. Stoller, A. Velamakanni, R.D. Piner, R.S. Ruoff, Carbon 48 (2010) 2118-2122.

[43] L.J. Cote, R. Cruz-Silva, J.X. Huang, J. Am. Chem. Soc. 131 (2009) 11027-11032.

[44] M.F. El-Kady, V. Strong, S. Dubin, R.B. Kaner, Science 335 (2012) 1326-1330.

[45] W. Gao, N. Singh, L. Song, Z. Liu, A.L.M. Reddy, L.J. Ci, R. Vajtai, Q. Zhang, B.Q. Wei, P.M. Ajayan, Nat. Nanotechnol. 6 (2011) 496-500.

[46] J.Y. Luo, H.D. Jang, J.X. Huang, ACS Nano 7 (2013) 1464-1471.

[47] M.D. Stoller, S.J. Park, Y.W. Zhu, J.H. An, R.S. Ruoff, Nano Lett. 8 (2008) 3498-3502.

[48] C.G. Liu, Z.N. Yu, D. Neff, A. Zhamu, B.Z. Jang, Nano Lett. 10 (2010) 4863-4868.

[49] K.X. Sheng, Y.Q. Sun, C. Li, W.J. Yuan, G.Q. Shi, Sci. Rep.-Uk 2 (2012) 247. http://dx.doi.org/10.1038/srep00247.

[50] J.Y. Luo, J. Kim, J.X. Huang, Acc. Chem. Res. 46 (2013) 2225-2234.

[51] Z.H. Bao, M.R. Weatherspoon, S. Shian, Y. Cai, P.D. Graham, S.M. Allan, G. Ahmad, M.B. Dickerson, B.C. Church, Z.T. Kang, H.W. Abernathy, C.J. Summers, M.L. Liu, K.H. Sandhage, Nature 446 (2007) 172-175.

[52] W. Luo, B. Wang, X.F. Wang, W.F. Stickle, X.L. Ji, Chem. Commun. 49 (2013) 10676-10678.

[53] A. Chakrabarti, J. Lu, J.C. Skrabutenas, T. Xu, Z.L. Xiao, J.A. Maguire, N.S. Hosmane, J. Mater. Chem. (2011) 9491-9493.

[54] H.L. Poh, Z. Sofer, J. Luxa, M. Pumera, Small 10 (2014) 1529-1535.

[55] A. Dabrowska, A. Huczko, S. Dyjak, Phys. Status Solidi B 249 (2012) 2373-2377.

[56] H.T. Zhang, X. Zhang, X.Z. Sun, D.C. Zhang, H. Lin, C.H. Wang, H.J. Wang, Y.W. Ma, ChemSusChem (2013) 1084-1090.

[57] H.T. Zhang, X. Zhang, X.Z. Sun, Y.W. Ma, Sci. Rep.-Uk 3 (2013) 3534. http://dx.doi.org/10.1038/srep03534.

[58] Y.X. Xu, K.X. Sheng, C. Li, G.Q. Shi, J. Mater. Chem. 21 (2011) 7376-7380.

[59] X. Huang, Z.Y. Zeng, Z.X. Fan, J.Q. Liu, H. Zhang, Adv. Mater. 24 (2012) 5979-6004.

[60] P. Simon, Y. Gogotsi, Acc. Chem. Res. 46 (2013) 1094-1103.

Zhenyu Xing received a B.Sc. degree from the Department of Chemistry of Jilin University in 2012. He joined the Department of Chemistry of Oregon State University in 2012 as a Ph.D. student and is currently working on metallothermic reactions and nanoporous graphene for energy storage.

Dr. Bao Wang received B.S. (2004), M.S. (2007) at University of Science and Technology Liaoning, and his Ph.D. at Institute of Chemistry, Chinese Academy of Sciences. He worked as Postdoctoral fellow at Nanyang Technological University (2011-2013) and Oregon State University (2013-2014). He is currently a Senior Researcher at Seoul National University (2014-present).

Wen-Yang Gao was born in Shandong, China in 1989. He received his B.Sc. degree with honors from Sun Yat-sen University, China in 2011. During his undergraduate years, he carried out metal-organic framework research under the supervision of Dr. Long Jiang and Dr. Tong-Bu Lu. In the fall of 2011, he joined the research group of Professor Shengqian Ma to pursue his Ph.D. degree at the University of South Florida. His research focuses on the development of functional porous materials for energy-related applications, including porous metalloporphyrin-based materials, CO_2 capture and fixation.

Changqing Pan was born in Lianyungang in 1979 and received his B.Sc. degree from Zhejiang University and M.Sc. degree from the University of Alabama. He is a chemical engineering Ph.D. student in Oregon State University and is currently working on process and characterization of materials for energy storage and conversion.
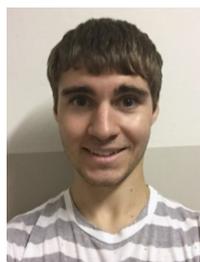
Josh Halsted is a second year undergraduate student at Oregon State University, majoring in nuclear engineering. He has been a part of Dr. Ji's research group from January 2014 until October 2014, mentored by Zhenyu Xing during that time period. He is a member of the Alpha Tau Omega fraternity, Alpha Sigma chapter and the Sophomore Representative for the American Nuclear Society (ANS) chapter at OSU. Mr. Halsted has interests in energy production, rocket science, particle physics, and a possible graduate degree in chemical engineering.

Elliot Chong is an undergraduate student at Oregon State University, majoring in General Science with the option of Pre-Pharmacy. He has completed his first scientific research regarding nanoporous graphene and will continue to work on metallothermic reactions.

Dr. Jun Lu is currently a scientist in Argonne National Laboratory. He was a DOE-EERE postdoctoral fellow under Vehicles Technology Program. His research interests focus on the electrochemical energy storage and conversion technology, with main focus on beyond Li-ion battery technology. Dr. Lu earned his bachelor degree in Chemistry Physics from University of Science and Technology of China (USTC) in 2000. He completed his Ph.D. from the Department of Metallurgical Engineering at University of Utah in 2009 with a major research on metal hydrides for reversible hydrogen storage application. Dr. Lu has authored/co-authored more than 70 peer-reviewed research articles and has filed over dozen patents and patent applications.
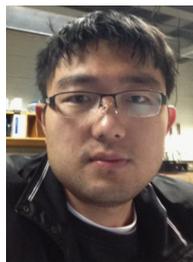
Xingfeng Wang received his B.Sc. degree from Jilin University in China in 2012. Since September 2012, he has been a Ph.D. student in Dr. Ji's group in Oregon State University. His research interest focuses on new electrochemical principles and their applications in supercapacitors.

Dr. Wei Luo received his B.E. (2006) and M.E. (2009) from Northwestern Polytechnical University and then obtained his Ph.D. from Huazhong University of Science and Technology in 2012 under the supervision of Professor Xianluo Hu and Professor Yunhui Huang. He worked with Professor Xiulei (David) Ji from 2012 to 2014 at Oregon State University. He is currently a postdoctoral fellow at the University of Maryland. His research focuses on new materials and their properties on energy storage and conversion.

Dr. Chih-hung (Alex) Chang is currently a Professor in the School of Chemical, Biological, and Environmental Engineering at the Oregon State University. His group has studied solution based thin film deposition processes, ink jet printing, microreaction technology and nanomaterials. His research group was one the first to report inkjet printing amorphous oxide TFTs and CIGS solar cells. Microreactor-Assisted Nanomaterial Deposition, MAND, a technique that was developed jointly by his group, was recognized by the Society of Manufacturing Engineers as the 2011 SME "Innovations That Could Change the Way You Manufacture" Watch List. Chih-hung is a SHARP Labs of America scholar, an Intel Faculty Fellow, and a recipient of AVS Graduate Research award, National Science Foundation's CAREER award, and awardees of W.M. Keck Foundation. He is the founder and Director of Oregon Process Innovation Center, an Oregon BEST signature research lab. He is a co-founder of a start-up venture, CSD Nano Inc. He has more than 100 refereed publications, 10 issued patents, and 3 pending patents.

Dr. Youhai Wen is a Materials Research Engineer with the National Energy Technology Laboratory. He has 15+ years of research experience in computational materials science and is currently leading a multi-year program entitled 'Alloy Modeling and Life Prediction' that develops physics-based multiscale oxidation modeling approach for metal systems and quantitative microstructural evolution modeling in multicomponent commercial alloy systems including Ni-base superalloys.
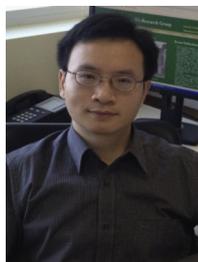
Dr. Shengqian Ma received his B.S. degree from Jilin University, China in 2003, and graduated from Miami University (Ohio) with a Ph.D. degree under the supervision of Hong-Cai Joe Zhou (currently at Texas A&M University) in 2008. After finishing two-year Director's Postdoctoral Fellowship at Argonne National Laboratory, he joined the Department of Chemistry at University of South Florida as an Assistant Professor in August 2010. His current research interest focuses on the development of functional porous materials for energy, biological, environmental-related applications.

Dr. Khalil Amine is a Distinguished Fellow and the Manager of the Advanced Battery Technology programs at Argonne National Laboratory, where he is responsible for directing the research and development of advanced materials and battery systems for HEV, PHEV, EV, satellite, military and medical applications. Dr. Amine currently serves a member of the U.S. National Research Consul on battery related technologies. Among his many awards, Dr. Khalil is a 2003 recipient of Scientific America's Top Worldwide Research 50 Research Award, a 2009 recipient of the US Federal Laboratory Award for Excellence in Technology Transfer, and is the four-time recipient of the R&D 100 Award, which is considered as the Oscar of technology and innovation. In addition, he was recently awarded the ECS battery technology award and the international battery association award. Dr. Amine holds or has filed over 130 patents and patent applications and has over 280 publications. From 1998-2008, Dr. Amine was the most cited scientist in the world in the field of battery technology.

Dr. Xiulei (David) Ji received his B.Sc. Degree from Jilin University in 2003. He obtained his Ph.D. in 2009 from Professor Linda Nazar's group at the University of Waterloo. From 2010 to 2012, sponsored by the NSERC Postdoctoral Fellowship, Xiulei worked with Professor Galen D. Stucky at the University of California, Santa Barbara. Since 2012, Xiulei leads a research group at Oregon State University. His current research interest is to explore basic synthetic materials chemistry and new electrochemical principles for energy storage purposes.